



Protein Science

**Estimate your dose: RADDOSE-3D**

Journal:	<i>Protein Science</i>
Manuscript ID	PRO-17-0232.R1
Wiley - Manuscript type:	Tools for Protein Science
Date Submitted by the Author:	n/a
Complete List of Authors:	Bury, Charles; University of Oxford, Department of Biochemistry Brooks-Bartlett, Jonathan; University of Oxford, Department of Biochemistry Walsh, Steven; University of Oxford, Department of Biochemistry Garman, Elspeth; University of Oxford, Department of Biochemistry
Keywords:	dose, radiation damage, beam profile, absorption coefficients, diffraction weighted dose

SCHOLARONE™  
Manuscripts



## Estimate your dose: RADDPOSE-3D

Charles S. Bury, Jonathan C. Brooks-Bartlett, Steven P. Walsh and Elspeth F. Garman\*

Department of Biochemistry, South Parks Road, Oxford OX1 3QU

\*Corresponding author

Abstract:

We present the current status of RADDPOSE-3D, a software tool allowing the estimation of the dose absorbed in a macromolecular crystallography diffraction experiment. The code allows a temporal and spatial dose contour map to be calculated for a crystal of any geometry and size as it is rotated in an X-ray beam, and gives several summary dose values: among them diffraction weighted dose. This allows experimenters to plan data collections which will minimise radiation damage effects by spreading the absorbed dose more homogeneously, and thus to optimise the use of their crystals. It also allows quantitative comparisons between different radiation damage studies, giving a universal 'x-axis' against which to plot various metrics.

Keywords: dose, radiation damage, beam profile, absorption coefficients, diffraction weighted dose

### Introduction

Radiation damage inflicted during X-ray diffraction experiments has plagued macromolecular crystallography (MX) since the early days of the field. Tracking its effects, either in reciprocal space from the diffraction images or in real space from the final electron density maps, requires a generally used and reproducible 'x-axis' against which to plot the various metrics used to monitor radiation damage. Parameters such as time, image number or goniometer angle are not useful for comparative studies between experiments, nor for obtaining knowledge on the radiation damage progression rates under different experimental conditions and data collection protocols.

A quantity that can fulfill the need for a universally applicable x-axis for this purpose is the absorbed dose  $D$ . This is defined as the energy absorbed per unit mass of sample during irradiation, in SI units of gray (Gy = J/kg). It is generally accepted that the rate of damage in a protein crystal is proportional to the dose (with certain caveats –see later) as first observed in 1962 by Blake and Phillips (4) at room temperature (RT): the absorbed X-ray energy is dissipated in the protein and solvent, causing ionisation of atoms and sometimes bond breakage. Dose cannot be measured, but it can be estimated using knowledge of the incident beam characteristics (energy, flux, size and two-dimensional profile) and of the crystal characteristics (volume, morphology, unit cell size, protein atomic contents, number of amino acids, and solvent composition) as well as the exposure time per image and number of images. The crystal parameters allow the absorption coefficients for X-rays to be calculated, permitting the estimation of the absorbed dose.

Having defined the x-axis as dose,  $D$ , various radiation damage indicators can be defined to plot on the y-axis. In reciprocal space, the two most commonly used metrics are: the diffraction intensity of the  $n^{\text{th}}$  dataset, or wedge of data divided by the summed mean intensity of the first dataset or wedge,  $I_n/I_1$ , which decreases with dose, with higher resolution reflections fading first (40), and secondly  $B_{rel}$  defined as the  $B$ -factor of the 1<sup>st</sup> dataset subtracted from the  $B$ -factor of the  $n^{\text{th}}$  dataset,  $B_n - B_1$ . The gradient of this plot gives a sensitivity measure,  $s_{AD} = \Delta B_{rel} / 8\pi^2 \Delta D$ , typically around 0.012 Å<sup>2</sup>/MGy for cryocooled crystals held at around 100 K during data collection ((23). Among other possible y-axis metrics is  $R_d$  (14), which is defined as the  $R$ -factor between symmetry related reflections plotted not against the dose, but against the difference in the dose at which the



reflections were recorded,  $\Delta D$ . The  $R$ -factor tends to increase with  $\Delta D$  if the crystal is suffering radiation damage. Note that the three metrics described above do not necessarily give the same results when compared for, e.g., efficacy of scavengers in reducing radiation damage rates (12).

Mosaicity also tends to increase with dose, as does the unit cell volume, whereas  $I/\sigma(I)$  decreases. However, it has been shown that none of these are robust or reproducible metrics, and thus they do not tend to be commonly used (26; 37)

At the X-ray beam energies,  $E_x$ , routinely used in MX (7 keV to 15 keV), the basic interaction processes which occur on irradiation of a protein crystal can be divided into three mechanisms (see Figure 1). The first is diffraction (the Thomson effect), involving elastic scattering events during which no energy is lost on the crystal and thus no dose is absorbed. The second is the Compton effect resulting in inelastic scattering events in which the outgoing photon has a longer wavelength (and lower energy) than the incident one, with the residual energy being deposited in the crystal. The third one is the photoelectric effect in which the photon is totally absorbed by an atom, and a so-called 'photoelectron' is ejected, carrying with it the incident photon energy minus the binding energy of the electron to the atom. For a 12.4 keV (1 Å) absorbed X-ray, as many as 500 ionisation events in the crystal can be subsequently initiated by each original photoelectron (31). On ejection of the photoelectron, the atom is left in an excited state with a vacancy in one of its electron orbitals. The de-excitation occurs by an electron dropping from an outer shell to fill the hole, with the accompanying release of the difference in binding energy either by emission of an Auger electron or a fluorescent X-ray. For light elements the Auger process dominates, but the probability of fluorescent escape increases markedly with atomic number, being for example 30% for iron atoms. At  $E_x=12.4$  keV, ~98% of the beam goes through a 100 µm thick crystal (if it contains no non-organic atoms) without any interaction occurring, and of the 2% that does interact, 8% diffracts, 8% undergoes Compton scattering and 84% causes photoelectric emission: thus this latter effect accounts for >90% of the energy absorption, and thus for the dose (17).

There is a limit to the dose that can be tolerated by biological samples before their integrity is compromised. For instance, radiotherapy for human glioblastoma multiforme brain tumours is 60 Gy at 2 Gy/day for 30 days directed to the affected area, and this is the maximum dose ever medically delivered to humans, and small rodents will die in minutes if they absorb 1 kGy in a single dose. For protein crystals, Henderson (19) postulated a dose limit for MX from observations made in electron diffraction experiments at 77 K, and considered the relative energy loss in organic material when irradiated with 100 keV electrons compared with 8 keV photons. He suggested that protein crystals in MX would lose half their diffraction intensity following absorption of 20 MGy, the so-called 'Henderson limit'. This dose to half intensity,  $D_{1/2}$ , for MX was experimentally measured to be 43 ( $\pm 0.4$ ) MGy by Owen *et al* (34) who using a homogeneous ('top-hat') profile beam, monitored diffraction intensity loss between 20 and 2.2 Å in holo- (1 iron atom/2 amino acids) and apo- (no iron) ferritin crystals, whose absorption coefficients vary by more than a factor of 2 (1.113 mm<sup>-1</sup> compared to 0.406 mm<sup>-1</sup> respectively at  $E_x=12.7$  keV). However, it was found that at  $D_{1/2}$ , the final electron density maps derived for the data exhibited significant damage to particular amino acids ('specific damage') and a more conservative experimental limit of 30 MGy, corresponding to a diffraction intensity of  $0.7 \times I_1$ , was recommended (34). To plan an MX experiment below this dose limit, the dose must be estimated, and it was to facilitate this conveniently for crystallographers that the original RADDOSE programme was conceived and designed.

Note that the dose is a metric which takes account of the physical processes pertinent when X-rays traverse a crystal but does not include possible chemical effects related to the true atomic



environment, and these may result in the crystal not reaching the dose limit. For example, certain amino acids such as aspartates and glutamates are known to be particularly susceptible to specific damage, and if they are present at crystal contacts, the lattice may break down well before the dose limit is reached (as reported in (28)). In addition, in principle radical scavengers can be either co-crystallised with, or soaked into the crystal to modify the radiation chemistry taking place, and a number of studies have tested this method of extending macromolecular crystal lifetime both at 100 K and RT. The results from various research groups disagree, with conflicting publications as to the efficacy of this strategy (see for example the results in (11) compared with (24) for sodium nitrate at 100 K, and those in (22) vs (30) for nicotinic acid). However, none of the tested scavengers has resulted in more than a factor of 2 increase in dose tolerance, with the exception of 1,4 benzoquinone which improved the dose lifetime of RT lysozyme crystals by a factor of >9 (3). Table 1 and the Supplementary Table of (1) summarise all the results on scavengers for MX up to 2013, and to the authors knowledge, there have been no additional studies since then apart from that of (10) on uridine as a radical scavenger for both MX and SAXS.

### RADDOSE v1-3

RADDOSE v1 (27) was written at a time when typical X-ray beams were larger than most protein crystals. It could thus take the incident flux (photons/sec) multiplied by the data collection time as the total flux impinging on the crystal, and treat the crystal as static in the beam to calculate the absorbed dose. The FORTRAN77 code was dependent on parts of the CCP4 software suite (41) for space group information, and reported the maximum dose absorbed. The Thomson (elastic), Compton (inelastic) and photoelectric effect cross sections were obtained from those compiled in reference (25), and accessed from the '*muca*' subroutine (2) incorporated into RADDOSE. All three processes were used to calculate the attenuation cross section ( $\mu_{att}$ ), but the Compton cross section was not included in the absorption coefficient ( $\mu_{abs}$ ) for the dose calculation. Additionally, fluorescent X-rays emitted by heavier mass atoms were assumed to be absorbed within the crystal, so were all included in the energy loss computation.

The dose,  $D$ , was calculated according to the following formula:

$$D \propto \frac{I_0}{\lambda V} [1 - \exp(-\mu_{abs} t)] \quad \text{and} \quad \mu_{abs} = \frac{1}{V} \sum_{j=1}^N \sigma_{pe}$$

where  $I_0$  is the incident beam flux,  $\lambda$  is the wavelength of the beam,  $V$  is the irradiated crystal volume,  $t$  is the crystal thickness, and  $\sigma_{pe}$  is the photoelectric cross section summed over the various atomic constituents of the crystal in the correct proportions (1... $N$ ). DNA and RNA as well as protein could be included in the calculation.

For the convenience of the user, solvent concentrations could be entered as mM quantities. The beam could be either a Gaussian with user defined horizontal and vertical full width half-maxima (FWHM), or a homogeneous 'top-hat' in profile. In order to improve the cross section accuracy for heavier atoms, RADDOSE v1 could read in a fluorescent scan collected over an absorption edge at a synchrotron beamline: this scan was pre-processed with the software program CHOOCH (15). Crystal morphology could only be specified as cuboid.

The program was distributed on request and the necessary information for running the program, in particular the flux, gradually became more available at MX beamlines. It was incorporated into the beamline programs BEST (5) and Web-Ice (18) to assist experimenters to design optimum data collection strategies. An analysis of the parameters affecting the absorbed dose using RADDOSE concluded that the dose was almost independent of the crystal thickness, since



the beam attenuation at the incident energies usually employed is negligible. However, reliable values for the beam area, profile and flux are a prerequisite for obtaining accurate dose estimates (28). Systematic flux calibration procedures were thus also established (33). Typical fluxes on modern synchrotron beamlines used for MX are, for example,  $3 \times 10^{12}$  ph/s on MASSIF-1 at the ESRF in Grenoble into a  $100 \mu\text{m}$  (h)  $\times$   $65 \mu\text{m}$  (v) FWHM Gaussian beam, and  $2 \times 10^{11}$  ph/s for P14 at PETRA III in Hamburg, for a defocused 'top-hat' shaped beam of  $140 \mu\text{m} \times 140 \mu\text{m}$ . At microbeam lines, the flux density is higher, for instance  $3 \times 10^{12}$  ph/s at I24 at the Diamond Light Source (DLS), UK for a  $6 \mu\text{m}$  (h)  $\times$   $9 \mu\text{m}$  (v) FWHM Gaussian beam. At XFELs, there are typically  $10^{12}$  photons in around a  $2 \mu\text{m}$  diameter beam pulse lasting 50 fs.

In the next iteration of the program, RADDOS v2 (36), the probability of any fluorescent X-rays escaping from the crystal following photoelectron emission from a heavier atom (see above) was included in the code, by including the ionisation probabilities for all atomic K, L and M shells, and the values for proportions of Auger and fluorescence production for all elements. To simplify the estimation of how many fluorescent photons were likely to escape, it was assumed that they were all produced in a plane perpendicular to the beam half way through the crystal. As an example, for a crystal of a 45 kDa protein with 10 Se-substituted methionines, the calculated dose at the Se edge (12.6634 keV) was reduced by 27% when fluorescent escape from the selenium was taken into account. This in turn extends the time taken to reach the dose limit of 30 MGy by 27%. Additionally, in RADDOS v2, the dependence on the CCP4 suite was removed. This version of the code was widely distributed to over 150 different researchers, and was also incorporated into a new version of BEST (6) and into EDNA (21).

In Version 3 (v3) of RADDOS (35), the Compton cross section was included in the absorption coefficient and the average Compton electron energy was computed by integration of the formula for their angular distribution. It was assumed that the inelastically scattered X-ray escapes from the crystal and the Compton electron was absorbed. The results showed that inclusion of this effect had negligible impact on dose values for incident X-ray energies below 20 keV. The Compton scattering cross section rises with incident energy, and the diffraction cross section decreases, as does that of the photoelectric effect. The relevant quantity for MX is the diffracted intensity per absorbed dose, which changes very little as the incident photon energy is increased. This version of the code was only distributed to experimenters using high incident energies, since at low energies the dose values were unchanged by the inclusion of Compton scattering.

### Need for RADDOS-3D

As the X-ray beams used for MX became smaller and microbeams became available at many synchrotrons (e.g. FWHM Gaussian beams at ID23-2, ESRF of  $10 \mu\text{m}$  (h)  $\times$   $4 \mu\text{m}$  (v) and as mentioned above, at I24, DLS of  $6 \mu\text{m}$  (h)  $\times$   $9 \mu\text{m}$  (v) with fluxes of  $1.1 \times 10^{12}$  ph/s and  $3 \times 10^{12}$  ph/s respectively), crystals were routinely larger than incident beams and were thus no longer completely bathed in it. Thus the dose values computed via the treatment used in RADDOS v1-3 became increasingly unsuitable, since as the crystal was rotated, new unexposed volume was being brought into the beam. It was clear that a completely new approach was required which would give temporal and spatial information of the absorbed dose in order to aid experimental protocol optimisation.

Concomitant with this issue was the question of which dose value should be quoted, since for a crystal rotated in a Gaussian beam, the maximum dose absorbed at the peak of the beam can be as much as 2 orders of magnitude greater than in parts of the crystal nearer to the tails of the beam. For example, for a cuboid shaped protein crystal ( $\mu_{\text{abs}} = 2.37 \text{ mm}^{-1}$ ) with  $100 \mu\text{m}$  sides in an uncollimated beam with a  $20 \times 20 \mu\text{m}$  FWHM 12.4 keV beam of flux  $5 \times 10^{11}$  ph/s, for a  $90^\circ$  wedge with a total of 60 s exposure, the maximum dose is 30.3 MGy (i.e. above the dose limit), but the average dose (whole crystal) is only 1.5 MGy.



Thus quoting the maximum dose did not give a realistic picture of how damaged the crystal was likely to be at the end of the experiment. It was thus beneficial to develop a metric that is more intimately linked to the diffraction pattern as the data collection proceeds (see below).

As mentioned above, a minor issue with RADDOSSE v1-3 was that the calculation of the beam attenuation as the beam traversed the crystal used the absorption coefficient,  $\mu_{abs}$ , rather than the attenuation coefficient,  $\mu_{att}$ , so did not account for the decrease in beam intensity due to the diffracted component of the interaction with the crystal. The effect of this assumption is only slight, since the majority of beam attenuation is due to the absorption component rather than diffraction (typically 92% versus 8% at 12.4 keV beam energy for a 100  $\mu\text{m}$  thick heavy atom free protein crystal).

### RADDOSSE-3D

The new RADDOSSE-3D code (44) was designed to allow easy extensibility so that new experimental scenarios can be included as they arise. It is highly modular so that future contributions from the community can be easily integrated into it. The language chosen for RADDOSSE-3D was Java, and the code follows an object-oriented programming architecture. In this programming paradigm, concepts are described by classes and their attributes. Objects are instances of such classes, which can be used to represent a part of the actual experiment, such as the crystal, the X-ray beam, and angular wedges of X-ray exposure. The crystal volume is partitioned into a set of evenly spaced three-dimensional voxel coordinates, each of finite volume, at which X-ray fluence (photons/second) and dose values are stored during the simulation. The granularity of the crystal can be user-defined to ensure that the simulation resolution is appropriate for the dimensions of the irradiated crystal. The distribution of dose within the crystal volume is calculated for a number of iterations in small angular steps across one or more data collection wedges, thus providing a three dimensional and time-resolved simulation of the dose state of the crystal. Multi-wavelength anomalous dispersion experiments can be specified, as usually the same crystal is used for the data collections at different incident energies.

A flow chart for RADDOSSE-3D is shown in Figure 2, and a representative input file is given in Figure 3. The program contains over 17,000 lines of functional Java code, and the job defined by the Figure 3 input file would take approximately 2 seconds to run on a 2 GHz Intel Core i5 processor.

Since the original publication describing RADDOSSE-3D, there have been a number of additions and improvements made to the code. Among these is the ability to input real experimental beam shapes for use in the calculation. The example input shown in Figure 3 uses different beam profiles for the 2 wedges of data (multiple wedges can be specified) defined by the user: a Gaussian shaped beam for the first and an experimentally measured beam profile for the second (a homogeneous 'top-hat' profile can also be specified). Beam profiles can be measured experimentally at a beamline using a variety of methods (scintillator images, aperture or line scans etc.). These measurements can be processed and transformed into portable graymap (.pgm) files, which can be input and interpreted by RADDOSSE-3D for the simulation of the experiment.

A further major addition to the code has been the incorporation of a way to specify an irregular crystal shape: previously the shapes that could be specified were confined to a cuboid or a sphere. For this, the three-dimensional geometry of the crystal is defined by its vertices and connecting edges in the OBJ geometry definition format. The generated polyhedron shape can be input into RADDOSSE-3D, and the program performs ray-tracing operations to determine the crystal interior and thus to define positions where voxels should be assigned. An external open-source software program, Blender (<https://www.blender.org>), provides an easy interface for creating arbitrary crystal shapes and generates geometry files that can be read directly into RADDOSSE-3D.



For convenience, if the protein structure for the irradiated crystal is already known, the PDB code can now be entered by the user and read into RADDOSSE-3D directly.

Other minor modifications have included firstly a better calculation of the volume in the unit cell occupied by RNA and DNA by setting their average densities to be the same as that of protein (1.3mg/ml), secondly the absorption calculation subroutine '*muca*' has been converted from Fortran into Java code to end any dependence of RADDOSSE-3D on RADDOSSE v2, and thirdly the attenuation coefficient (which includes the diffraction cross section) is now used to calculate the incident flux on the face of a voxel, rather than using the absorption coefficient (see above).

Using RADDOSSE-3D, the dose distributions for various data collection protocols can be usefully explored (43) in order to spread the absorbed dose as homogeneously as possible over the full crystal volume. It is important to note here that inhomogeneous irradiation results in the crystal having a range of site specific damage states at any instant, and thus the electron density derived from the data will be an average of all these states. Thus it is highly desirable to irradiate the crystal as evenly as possible. For example, for beams smaller than the crystal, the crystal can be rotated in the beam around a single axis as is traditionally employed (Figure 4(a)), or it can be translated after a certain angular wedge has been collected resulting in a dose map that is colloquially referred to as a 'Newton's cradle' (Figure 4(b)) or it can be simultaneously translated and rotated (Figure 4(c), the so called 'helical data collection' (16)), resulting in a spiral path along a needle shaped crystal. Another possible strategy is to deliberately displace the centre of the crystal from the spindle rotation axis, giving a 'doughnut' shaped dose contour (Figure 4(d)) which reduces the maximum dose and has been experimentally shown to give better quality data and a longer crystal lifetime in the beam (42). This latter approach can be combined with the helical strategy to further spread the dose (Figure 4(e)). An intrinsic assumption in the discussion above is that the rate of radiation damage in MX is proportional to the absorbed dose and is not dose rate dependent. This relationship is still believed to be true for experiments carried out at cryo-temperatures, but has been questioned for high dose rate RT measurements, where a ~100ms 'lag period' has been observed before a decrease in diffraction intensity becomes apparent (32). In addition, at low dose rates, damage rates at RT that are inversely proportional to the dose rate have been documented (39). Thus there is current debate concerning the relationship between dose rate and damage rates at RT.

The effect on the dose distributions of using various Gaussian FWHM beam profiles with the same flux (but thus different flux densities) is illustrated for an irregular shaped crystal of volume  $10^6 \mu\text{m}^3$  in Figure 5. As expected, it can be seen that the  $20 \mu\text{m} \times 20 \mu\text{m}$  profile gives the biggest dose contrast, and it is clear that parts of the crystal are not used at all, whereas data collection with the  $50 \mu\text{m} \times 50 \mu\text{m}$  beam results in a more even dose distribution. The most homogeneous distribution is achieved with a 'top-hat' beam (Fig 5d)).

As can be seen from Figure 4, there is usually a large range of absorbed doses within a crystal by the end of an MX experiment. RADDOSSE v1-3 quoted the maximum dose (MD) in the sample, which for a Gaussian shaped beam incident on a centred crystal is usually in the centre. This value does not give an indication of the average dose absorbed by the irradiated part of the crystal, or an idea of the current state of the diffracting power. Thus we proposed the introduction of a metric, the Diffraction Weighted Dose (DWD), which combines information on the cumulative dose within each volume element of the crystal up to a given time, weighted by the fluence through that voxel at that instant. This metric has been described in detail previously, and experimentally validated by showing that for 3 very different sized inhomogeneous beams, the DWD gave consistent results for the intensity decay and scaling *B*-factor rise for data collections on cubic insulin crystals (42). The dose values on the x-axis of all the figures shown here are the Diffraction Weighted Dose (DWD), calculated by RADDOSSE-3D.



The DWD metric has already been used to good effect in a mechanistic study of a co-factor free oxidase using a combination of on-line Raman and MX (8) and in an enzyme catalysis study of copper nitrite reductase (20). The necessity for the DWD metric is clear from the irradiation regimes shown in Figure 4(a), where there is a significant difference between the MD (78.9 MGy) and the average dose (1.98 MGy) calculated over the entire crystal volume. The DWD is 10.0 MGy, demonstrating how the MD and average dose significantly over- and underestimate the relevant accumulated dose, respectively, which propagates through to the recorded diffraction data.

In addition, whereas the average dose for both strategies in Figures 4(a) and 4(c) is 1.98 MGy (as calculated over the whole crystal volume) the DWD is considerably lower for the crystal shown in Figure 4(c) compared with 4(a) (2.9 MGy versus 10 MGy), indicating the positive effect that crystal translation parallel to the rotation axis has to more efficiently spread the dose throughout the crystal volume. Again, in Figure 4(c), the max dose (11.6 MGy) overestimates the relevant accumulated dose, but to a lesser extent than in 4(a), as anticipated.

### RADDOSE-3D for SAXS

RADDOSE-3D was recently extended (7) to estimate the dose in a Small Angle X-ray Scattering (SAXS) experiment which uses an arrangement as illustrated in Figure 6 to determine the overall shape of macromolecules. The liquid protein solution in buffer is irradiated at room temperature in a cylindrical capillary made of glass or quartz. RADDOSE-3D takes account of this experimental setup allowing doses to be calculated for many SAXS experiments.

The module that allows RADDOSE-3D to model arbitrary crystal shapes has been used to implement cylindrical shapes for a SAXS sample. The X-ray beam has to travel through the capillary material before it interacts with the protein sample. The capillary thus attenuates the X-ray beam, hence the measured flux value at the sample position is slightly higher than the true flux on the sample. RADDOSE-3D now allows the user to specify parameters for the capillary such as its material and thickness so that the code can calculate the attenuation of the X-ray beam before it reaches the sample.

The final major modification allows RADDOSE-3D to calculate the absorption coefficients given a description of the liquid sample composition. The simulation defines a volume of liquid and estimates its contents given the protein concentration (provided by the user in mg/ml) and buffer composition. The molecular mass of the molecule is calculated either from the protein sequence file (the sample can also contain DNA and RNA) by summing the molecular mass of each residue in the file, or alternatively, an average molecular weight is used for each residue (110.0 Da for protein residues, 339.5 Da for RNA nucleotides and 327.0 Da for DNA nucleotides). The number of molecules in the volume can then be calculated and hence the absorption coefficient can be computed.

Using the resulting dose values, sample lifetimes can be compared across different facilities, and aggregation avoided by suitable experimental design. For instance, evaluation of putative scavengers can be quantitative rather than qualitative. In a recent such study (7), a range of threshold doses (above which the SAXS data were determined to be compromised) ranged between 2.37 and 51.24 kGy, much lower than typical values for the dose required to reduce the diffraction to half of its initial intensity ( $D_{1/2}$ ) determined for RT MX.

However, the program cannot yet handle cases where the sample is continuously flowed through the capillary during X-ray irradiation, a common strategy in SAXS to avoid radiation damaged data being collected.



### Other contributions to the absorbed dose value

Several other physical effects must be taken into account to obtain true estimates of the dose absorbed by a protein crystal, and a number of these have recently been incorporated into the RADDOS-3D code.

Firstly, RADDOS-3D has been modified to take into account the energy deposited in the crystal by electrons produced by the inelastic scattering of X-rays, the Compton effect. As mentioned above, this was taken into account in RADDOS v3, and found to make negligible difference to the dose values obtained for incident X-ray energies below 20 keV and very little difference below 40 keV. The Compton cross section increases only slowly in this energy region, concomitant with a steeper decrease in the photoelectric cross section. The parameterisation of the electron energy distribution implemented in RADDOS-3D is identical to that detailed previously (35).

Figure 7 shows a plot of DWD against X-ray energy for the same sample (sample smaller than beam) and data collection conditions with and without consideration of the Compton electron energy loss (CEEL). It can be seen that the results from RADDOS-3D concur with the conclusions drawn previously from the Raddos v3 results (35), i.e. that the effect is negligible for incident energies below 20 keV. Thus this modification of the code will only make a noticeable difference to DWD when higher energy incident beams are used, as noted by Cowan and Nave (9) from their analysis of CASINO simulations including the CEEL.

Secondly, as pointed out over a decade ago by Nave and Hill (29), for small crystals (less than around 10  $\mu\text{m}$  in size), there is a significant probability that the ejected photoelectron will escape from the crystal rather than depositing all of its energy within it. This effect will reduce the dose, and this implies that smaller crystals will have an extended lifetime in the beam compared with larger ones. Clearly, to take this effect into account, the range of the photoelectrons produced by different incident beam energies must be known, as well as some parameterisation of their energy loss as a function of penetration depth through the sample. We are currently incorporating this effect into RADDOS-3D, and following extensive simulations with CASINO ('monte Carlo Simulation of electron trajectory in solids') [<http://www.gel.usherbrooke.ca/casino/What.html>], we are now able to model these distributions analytically. The path length of photoelectrons of energy  $E$  has been found to approximately follow a Gumbel distributed random variable,  $X_{pe}$ , with Probability Density Function (PDF), for incident beam energies up to 20 keV:

$$PDF = \frac{1}{\beta} \exp[-(z + \exp(-z))] \quad \text{and} \quad z = \frac{(x-\mu)}{\beta}$$

where  $\mu$  is the mean path length of a photoelectron of a given energy, and  $\beta$  is an energy dependent scale parameter determined by a polynomial fitting to the results of CASINO simulations run for different incident energies. The validity of the Gumbel distribution was tested up to a beam energy of 30 keV, and up to  $E_x = 20\text{keV}$  the  $\beta$  parameter of the Gumbel distribution approximately followed the quadratic relationship:

$$\beta = 0.002 E_x^2 + 0.0096 E_x$$

This quadratic relationship is implemented in RADDOS-3D, and consequently should currently only be used for beam energies up to 20 keV.

In RADDOS-3D, for each crystal voxel, photoelectrons are then modelled to spread their kinetic energy along linear tracks of a randomly assigned length,  $X_{pe}(\text{voxel})$ , extending uniformly in all directions from the original voxel. If the linear track of a photoelectron exits the crystal boundary, all its remaining kinetic energy is then lost from the crystal. The effect of any beam polarisation on the preferential direction in which photoelectrons travel is not currently taken into account.

Experimentally, the range photoelectrons produced by an 18.7 keV beam has been measured through radiation damage studies with a 1  $\mu\text{m}$  sized beam, and found to be 4  $\mu\text{m}$  (38). Figure 8 shows the effect on the DWD at  $E_x = 12.4$  keV of taking the probability of photoelectron



escape into account for isolated crystals of various dimensions. It can be seen that for a 20  $\mu\text{m}$  crystal there is a dose reduction of about 3% whereas this rises to over 20% for a 10  $\mu\text{m}$  crystal. As the incident energy is increased, the probability of photoelectron escape will increase. An important caveat for the dose reduction described here is that for a crystal held within a cryoloop completely surrounded by vitrified cryobuffer which is also in the beam path, as many photoelectrons will enter the crystal from the buffer as will leave it, so there will be no concomitant reduction in the dose at all. Thus photoelectron escape modelling is only valid if the effects of the surrounding buffer are assumed to be negligible.

The effect described above is especially relevant when calculating the dose absorbed during X-ray Free Electron Laser serial crystallography experiments, where generally micro- or nano-crystals are utilised.

### **Future developments planned for RADDOS-3D**

Several further refinements of RADDOS-3D are planned, with the eventual aim of being able to use it to determine an optimum data collection strategy given information about the beamline geometry, the 2-D beam profile and the crystal shape. In particular, development of better protocols for imaging real experimental X-ray beam profiles and incorporation of online methods for determining the physical shape of macromolecular crystals would be beneficial. If these could be conveniently input directly into RADDOS-3D, dose estimates could be more reliable and thus useful. A question is often asked regarding the importance of knowing the exact crystal shape and size when running RADDOS-3D, and the effect on the resulting calculated dose if they are not accurately known. Figure 9 illustrates the variation in DWD when irregular crystal shapes (Figs 8a and 8b) are approximated by either a cuboid (Fig 8c) or a sphere (Fig 8d), for 4 very different crystal shapes all having the same volume (of  $10^6 \mu\text{m}^3$ ), and it can be seen that it lies between 9.4 and 10.3 MGy. Given other uncertainties in the experiment, these simulations show that knowing the exact crystal shape is not pivotal in obtaining a reasonable dose estimate.

As mentioned above, the probability of fluorescence rather than Auger electron emission following photoelectron ejection rises as the atomic number of the sample constituent increases: it is approximately 7% for sulphur, rising to 60% for selenium. These fluorescent X-rays then have a finite chance of escaping from the sample, carrying with them the binding energy of the photoelectron. This has the effect of reducing the dose for samples containing heavier atoms, and was taken into account in RADDOS v2 (36). It has yet to be incorporated into RADDOS-3D.

There is renewed interest in using pink beams ( $\Delta\lambda/\lambda > 0.5\%$ ) for MX (e.g. see (13)) and also for performing Laue experiments. Additionally, the band width of XFEL beams tends to be ( $\Delta\lambda/\lambda \sim 1.0\%$ ). Incorporating an energy spectrum for the incident beam into RADDOS-3D would thus allow dose calculations for these scenarios.

A very useful extension of RADDOS-3D would be to adapt it to give doses during electron microscopy (EM) experiments. Recent advances in this field have allowed far higher resolution macromolecular structural models than previously possible with EM, and have resulted in site-specific radiation damage effects being observed (R. Henderson, private communication). There is thus now interest in tracking this as a function of dose.

### **Code availability:**

RADDOS-3D is an open source software tool which can be freely accessed at [www.raddo.se](http://www.raddo.se) along with the User Guide, and the source code is also available for download at <https://github.com/GarmanGroup/RADDOS-3D>.



**Acknowledgements:**

We gratefully acknowledge all the people who have contributed to the development and coding of RADDOSSE v1-3: Raimond Ravelli, James Murray, Robin Owen, and Karthik Paithankar, and of RADDOSSE-3D: Oliver Zeldin, Markus Gerstel, Jean-Paul Ebejer, Helen Ginn, and Ben Gayther.

**Figure captions:****Figure 1**

Interaction processes of incident X-ray photon with atoms in the crystal. The photon cross-sections for each interaction (in units of barns/atom: 1 barn =  $10^{-28}$  m<sup>2</sup>) have been provided for C, S and Se, for an incident 12.4 keV (1 Å) X-ray beam, as reported in the XCOM Photon Cross Section Database (<http://physics.nist.gov/PhysRefData/Xcom/html/xcom1.html>).

**Figure 2**

Flow chart outlining the structure of RADDOSSE-3D.

**Figure 3**

The structure of a typical RADDOSSE-3D input file. The crystal geometry and composition is first described by a 'Crystal' block (in orange). The three-dimensional geometry of the crystal has been approximated as a polyhedron (as a collection of vertices and faces) and this information has been supplied to RADDOSSE-3D using the 'ModelFile' flag. A 'Beam' block (in blue) followed by a 'Wedge' block (in green) describe the strategy by which the specified beam will interact with the crystal. Multiple beam and wedge parameters can be implemented in the same RADDOSSE-3D input file, and each exposure strategy will be run sequentially by the program. Whereas in the first beam block the beam profile will be approximated as a 2D Gaussian with FWHMs of 20 µm x 20 µm, in the second beam block, the beam profile has been extracted directly from the beamline and supplied to RADDOSSE-3D as an input .pgm file.

**Figure 4**

Effect of the dose distribution on the chosen exposure strategy modelled in RADDOSSE-3D. Dose contouring levels have been shown at 0.0001 MGy (grey), 5 MGy (green), 10 MGy (light blue), 20 MGy (dark blue) and 30 MGy (red), using R ([www.r-project.org](http://www.r-project.org)). In each simulation, the crystal rotation axis (in black) and incident beam direction (in yellow, coincident with the z-axis) are shown. Unless otherwise stated, each dose distribution is generated following a 360° rotation over a total exposure time of 100 s. In (a) the crystal rotation axis and incident beam direction intersect. In (b) the crystal undergoes a series of eight 360° rotations, each lasting  $100/8 = 12.5$  s, intersected by a series of 20 µm translations of the crystal parallel to the rotation axis to spread the dose across the crystal volume. In (c) the crystal rotation axis and incident beam direction intersect, however the crystal is continuously translated along the rotation axis at a rate of 0.2 µm/°. In (d) the crystal rotation axis has been offset by 30 µm relative to the incident beam direction. In (e) the rotation axis is offset by 30 µm relative to the beam direction, and the crystal is also continuously translated along the rotation axis at 0.2 µm/°. In all simulations a cuboid crystal has been modelled with dimensions  $x = 100$  µm,  $y = 200$  µm and  $z = 100$  µm. The beam has been modelled as Gaussian shaped (FWHM: 20 µm x 20 µm), with energy 12.4 keV, flux  $5 \times 10^{11}$  ph/s, and a large 1 mm x 1 mm rectangular collimation in order to ensure the full crystal is continuously bathed in the beam for each simulation.



**Figure 5**

The effect of varying the incident beam profile on the dose distribution for an irregular polyhedron shaped crystal formed by distorting a cube of dimension  $(100\text{ }\mu\text{m})^3$  leaving the total volume the same at  $10^6\text{ }\mu\text{m}^3$ . In (a)-(c) the beam has been modelled as Gaussian shaped, and the FWHM has been varied as: (a)  $20\text{ }\mu\text{m} \times 20\text{ }\mu\text{m}$ , (b)  $40\text{ }\mu\text{m} \times 40\text{ }\mu\text{m}$  and (c)  $60\text{ }\mu\text{m} \times 60\text{ }\mu\text{m}$ . In (d) a uniform 'top-hat' shaped beam distribution has been modelled. All other beam parameters have been kept constant (energy: 12.4 keV, flux  $5 \times 10^{11}$  ph/s, rectangular collimation:  $200\text{ }\mu\text{m} \times 200\text{ }\mu\text{m}$ ). In all simulations the crystal has been exposed for 100 s throughout a  $360^\circ$  rotation about the  $y$ -axis (shown in each plot). The direction of incident beam with respect to the initial orientation of the crystal has been shown (green arrow). The crystal morphology has been specified with the 'Type Polyhedron' flag in the RADDOS-3D input file. Visualisation has been produced using the open source Paraview software package (<https://www.paraview.org>).

**Figure 6**

Diagram of a basic SAXS experiment. An X-ray beam (typical energies range between 7 and 12.5 keV) is incident on a protein SAXS sample. Commonly the sample volume exposed to the beam is between  $15 - 30\text{ }\mu\text{l}$ , with a protein concentration that usually ranges from  $0.5 - 10\text{ mg/ml}$ . The scattered radiation is collected on a detector. The symbol,  $q$  in the figure, is termed the momentum transfer and is defined as  $q = 4\pi \sin \theta / \lambda$  where  $\theta$  is half the scattering angle, and  $\lambda$  is the wavelength of the incident X-ray beam. The detector images that are generated from the experiment can be processed and analysed to determine the overall shape and size of the protein molecule in the SAXS sample.

**Figure 7**

The effect of Compton scattering on the calculated DWD (MGy) values for a  $100\text{ }\mu\text{m} \times 100\text{ }\mu\text{m} \times 100\text{ }\mu\text{m}$  cuboid crystal in RADDOS-3D with varying incident photon energy,  $E_x$  (keV). In all simulations, the beam has been modelled as Gaussian shaped with energy: 12.4 keV, flux:  $5 \times 10^{11}$  ph/s, FWHM:  $20\text{ }\mu\text{m} \times 20\text{ }\mu\text{m}$  and with a rectangular collimation size of  $100\text{ }\mu\text{m} \times 100\text{ }\mu\text{m}$ . In all simulations the crystal has been exposed for 100 s over a  $360^\circ$  rotation. Note the  $y$ -axis logarithmic scale.

**Figure 8**

The effect of accounting for photoelectron escape in RADDOS-3D on the calculated DWD (MGy) values for a various sized cubic shaped crystals. In all simulations, the beam has been modelled as Gaussian shaped with energy: 12.4 keV, flux:  $5 \times 10^{11}$  ph/s, FWHM:  $20\text{ }\mu\text{m} \times 20\text{ }\mu\text{m}$  and with a rectangular collimation size of  $100\text{ }\mu\text{m} \times 100\text{ }\mu\text{m}$ , and the crystal has been exposed for 100 s over a  $360^\circ$ . The PixelsPerMicron parameter in RADDOS-3D has been varied for the  $x$ -dimension of each crystal (between 0.5 and 10 pixels/ $\mu\text{m}$ ) to account for the diminishing size of the crystal.

**Figure 9**

The effect of modelled crystal geometry on the calculated DWD (MGy) values has been illustrated for four crystal shapes, each with a total volume of  $10^6\text{ }\mu\text{m}^3$ . Dose isosurfaces are contoured at 0.001 MGy (light blue), 20 MGy (dark blue) and 30 MGy (red), using R ([www.r-project.org](http://www.r-project.org)). In (a) and (b),



two irregular polyhedron-shaped crystals were generated using the open-source three-dimensional graphics software called Blender. In (c) and (d) the 'Type cuboid' and 'Type spherical' input file parameters to RADDOSE-3D have been used to model the crystal as a 100  $\mu\text{m}$  x 100  $\mu\text{m}$  x 100  $\mu\text{m}$  cuboid, and 124.2  $\mu\text{m}$  diameter sphere, respectively. In all simulations, a Gaussian beam (12.4 keV,  $1\text{e}11$  ph/s) was modelled with FWHM of 20  $\mu\text{m}$  x 20  $\mu\text{m}$ , in order to obtain the infamous 'fried egg' effect.

## References

1. Allan EG, Kander MC, Carmichael I, Garman EF (2013) To scavenge or not to scavenge, that is STILL the question. *Journal of Synchrotron Radiation* 20:23-36.
2. X-ray Absorption Cross Sections (McMaster) Tables. : 1995.
3. Barker AI, Southworth-Davies RJ, Paithankar KS, Carmichael I, Garman EF (2009) Room-temperature scavengers for macromolecular crystallography: increased lifetimes and modified dose dependence of the intensity decay. *Journal of Synchrotron Radiation* 16:205-216.
4. Blake CCF, Phillips DC. Effects of X-irradiation on single crystals of myoglobin. (1962) Proceedings of the Symposium on the Biological Effects of Ionising radiation at the Molecular Level. International Atomic Energy Agency, Vienna, pp. 183–191.
5. Bourenkov GP, Popov AN (2006) A quantitative approach to data-collection strategies. *Acta Crystallographica Section D: Biological Crystallography* 62:58-64.
6. Bourenkov GP, Popov AN (2010) Optimization of data collection taking radiation damage into account *Acta Crystallographica Section D: Biological Crystallography* 66:409-419.
7. Brooks-Bartlett JC, Batters RA, Bury CS, Lowe ED, Ginn HM, Round A, E.F. G (2017) Development of tools to automate quantitative analysis of radiation damage in SAXS experiments. *J Synchrotron Radiation* 24:63–72.
8. Bui S, von Stetten D, Jambrina PG, Prangé T, Colloc'h N, de Sanctis D, Royant A, Rosta E, Steiner RA (2014) Substrate–Dioxygen Configuration in a Cofactor-free Oxidase. *Angew Chem Int Ed Engl* 53:13710–13714.
9. Cowan JA, Nave C (2008) The optimum conditions to collect X-ray data from very small samples. *Journal of Synchrotron Radiation* 15:458-462.
10. Crosas E, Castellvi A, Crespo I, Fulla D, Gil-Ortiz F, Fuertes G, Kamma-Lorger CS, Malfois M, Arandaa MAG, Juanhuix J (2017) Uridine as a new scavenger for synchrotron-based structural biology techniques. *Journal of Synchrotron Radiation* 24:53-62.
11. de la Mora E, Carmichael I, Garman EF (2011) Effective scavenging at cryotemperatures: further increasing the dose tolerance of protein crystals. *Journal of Synchrotron Radiation* 18:346-357.
12. De la Mora E, Lovett JE, Blanford CF, Garman EF, Valderrama B, Rudino-Pinera E (2012) Structural changes caused by radiation-induced reduction and radiolysis: the effect of X-ray absorbed dose in a fungal multicopper oxidase. *Acta Crystallographica Section D: Biological Crystallography* 68:564-577.
13. Dejoie C, McCusker LB, Baerlocher C, Abela R, Patterson BD, Kunz M, Tamura N (2013) Using a non-monochromatic microbeam for serial snapshot crystallography. *Journal of Applied Crystallography* 46:791–794.
14. Diederichs K (2006) Some aspects of quantitative analysis and correction of radiation damage. *Acta Crystallographica Section D: Biological Crystallography* 62:96-101.
15. Evans G, Pettifer RF (2000) CHOOCH: a program for deriving anomalous-scattering factors from X-ray fluorescence spectra. *J Appl Cryst* 34: 82-86.
16. Flot D, Mairs T, Giraud T, Guijarro M, Lesourd M, Rey V, van Brussel D, Morawe C, Borel C, Hignette O, Chavanne J, Nurizzo D, McSweeney S, Mitchell E (2010) The ID23-2 structural



- biology microfocus beamline at the ESRF. *Journal of Synchrotron Radiation* 17:107-118. PMID: 20029119 {Medline}
17. Garman EF (2010) Radiation damage in macromolecular crystallography: what is it and why should we care? *Acta Crystallographica Section D: Biological Crystallography* 66:339-351. PMID: 20382986 {Medline}
  18. González A, Moorhead P, McPhillips S.E., Song J, Sharp K, Taylor JR, Adams PD, Sauter NK, Soltis SM (2008) Web-Ice: integrated data collection and analysis for macromolecular crystallography. *J Appl Cryst* 41:176-184.
  19. Henderson R (1990) Cryo-protection of protein crystals against radiation damage in electron and X-ray diffraction. *Proceedings of the Royal Society of London, Series B: Biological Sciences* 241:6-8.
  20. Horrell S, Antonyuk SV, Eady RR, Hasnain SS, Hough MA, Strange RW (2016) Serial crystallography captures enzyme catalysis in copper nitrite reductase at atomic resolution from one crystal. *IUCr*, 3:271-281.
  21. Incardona M-F, Bourenkov GP, Levik K, Pieritz RA, Popov AN, Svensson O (2009) EDNA: a framework for plugin-based applications applied to X-ray experiment online data analysis. *Journal of Synchrotron Radiation* 16:872-879
  22. Kauffmann B, Weiss MS, Lamzin VS, Schmidt A (2006) How to avoid premature decay of your macromolecular crystal: a quick soak for long life. *Structure (Camb)* 14:1099-1105.
  23. Kmetko J, Hussein NS, Naides M, Kalinin Y, Thorne RE (2006) Quantifying X-ray radiation damage in protein crystals at cryogenic temperatures. *Acta Crystallographica Section D: Biological Crystallography* 62:1030-1038.
  24. Kmetko J, Warkentin M, Englich U, Thorne RE (2011) Can radiation damage to protein crystals be reduced using small-molecule compounds? *Acta Crystallographica Section D: Biological Crystallography* 67:881-893. PMID: WOS:000295033700007 {Medline}
  25. McMaster WH, Del Grande NK, Mallett JH, Hubbell JH (1969) Compilation of x-ray cross sections. *Lawrence Livermore National Laboratory Report UCRL-50174*.
  26. Murray J, Garman E (2002) Investigation of possible free-radical scavengers and metrics for radiation damage in protein cryocrystallography. *Journal of Synchrotron Radiation* 9:347-354. PMID: 12409621 {Medline}
  27. Murray JW, Garman EF, Ravelli RBG (2004) X-ray absorption by macromolecular crystals: the effects of wavelength and crystal composition on absorbed dose. *Journal of Applied Crystallography* 37:513-522.
  28. Murray JW, Rudino-Pinera E, Owen RL, Grininger M, Ravelli RB, Garman EF (2005) Parameters affecting the X-ray dose absorbed by macromolecular crystals. *Journal of Synchrotron Radiation* 12:268-275.
  29. Nave C, Hill MA (2005) Will reduced radiation damage occur with very small crystals? *Journal of Synchrotron Radiation* 12:299-303.
  30. Nowak E, Brzuszkiewicz A, Dauter M, Dauter Z, Rosenbaum G (2009) To scavenge or not to scavenge: that is the question. *Acta Crystallographica Section D: Biological Crystallography* 65:1004-1006. PMID: WOS:000269350000015 {Medline}
  31. O'Neill P, Stevens DL, Garman EF (2002) Physical and chemical considerations of damage induced in protein crystals by synchrotron radiation: a radiation chemical perspective. *Journal of Synchrotron Radiation* 9:329-332. PMID: 12409618 {Medline}
  32. Owen RL, Axford D, Nettleship JE, Owens RJ, Robinson JI, Morgan AW, Dore AS, Lebon G, Tate CG, Fry EE, Ren J, Stuart DI, Evans G (2012) Outrunning free radicals in room-temperature macromolecular crystallography. *Acta Crystallographica Section D: Biological Crystallography* 68:810-818.
  33. Owen RL, Holton JM, Schulze-Briesse C, Garman EF (2009) Determination of X-ray flux using silicon pin diodes. *Journal of Synchrotron Radiation* 16:143-151. PMID: 19240326 {Medline}



34. Owen RL, Rudino-Pinera E, Garman EF (2006) Experimental determination of the radiation dose limit for cryocooled protein crystals. *Proceedings of the National Academy of Sciences, USA* 103:4912-4917. PMID: 16549763 {Medline}
35. Paithankar KS, Garman EF (2010) Know your dose: RADDOS. *Acta Crystallographica Section D: Biological Crystallography* 66:381-388. PMID: 20382991 {Medline}
36. Paithankar KS, Owen RL, Garman EF (2009) Absorbed dose calculations for macromolecular crystals: improvements to RADDOS. *Journal of Synchrotron Radiation* 16:152-162. PMID: 19240327 {Medline}
37. Ravelli RB, Theveneau P, McSweeney S, Caffrey M (2002) Unit-cell volume change as a metric of radiation damage in crystals of macromolecules. *Journal of Synchrotron Radiation* 9:355-360.
38. Sanishvili R, Yoder DW, Pothineni SB, Rosenbaum G, Xu S, Vogt S, Stepanov S, Makarov OA, Corcoran S, Benn R, Nagarajan V, Smith JL, Fischetti RF (2010) Radiation damage in protein crystals is reduced with a micron-sized X-ray beam. *Proceedings of the National Academy of Sciences, USA* 108:6127-6132.
39. Southworth-Davies RJ, Medina MA, Carmichael I, Garman EF (2007) Observation of decreased radiation damage at higher dose rates in room temperature protein crystallography. *Structure* 15:1531-1541. PMID: WOS:000251655400007 {Medline}
40. Teng T, Moffat K (2000) Primary radiation damage of protein crystals by intense synchrotron radiation. *Journal of Synchrotron Radiation* 7:313-317.
41. Winn MD, Ballard CC, Cowtan KD, Dodson EJ, Emsley P, Evans PR, Keegan RM, Krissinel EB, Leslie AG, McCoy A, McNicholas SJ, Murshudov GN, Pannu NS, Potterton EA, Powell HR, Read RJ, Vagin A, Wilson KS (2011) Overview of the CCP4 suite and current developments. *Acta Crystallographica Section D: Biological Crystallography* 67:235-242. PMID: 21460441 {Medline}
42. Zeldin OB, Brockhauser S, Bremridge J, Holton JM, Garman EF (2013) Predicting the X-ray lifetime of protein crystals. *Proceedings of the National Academy of Sciences, USA* 110:20551-20556. PMID: 24297937 {Medline}
43. Zeldin OB, Gerstel M, Garman EF (2013) Optimising the spatial distribution of dose in X-ray macromolecular crystallography. *Journal of Synchrotron Radiation* 20.
44. Zeldin OB, Gerstel M, Garman EF (2013) RADDOS-3D: time- and space-resolved modelling of dose in macromolecular crystallography. *Journal of Applied Crystallography* 46:1225-1230.



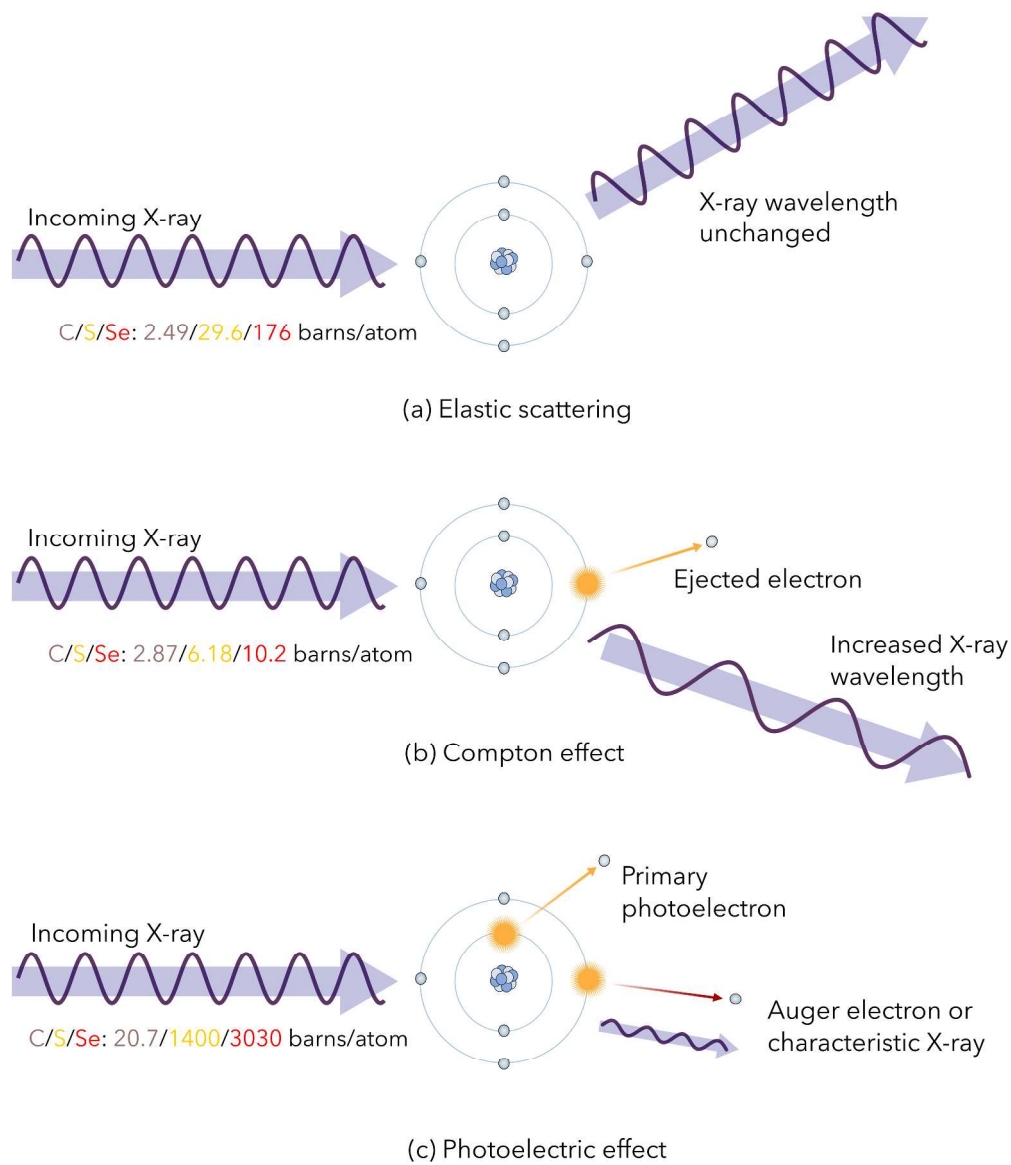


Figure 1  
Interaction processes of incident X-ray photon with atoms in the crystal. The photon cross-sections for each interaction (in units of barns/atom: 1 barn =  $10^{-28}$  m<sup>2</sup>) have been provided for C, S and Se, for an incident 12.4 keV (1 Å) X-ray beam, as reported in the XCOM Photon Cross Section Database (<http://physics.nist.gov/PhysRefData/Xcom/html/xcom1.html>).

277x319mm (300 x 300 DPI)



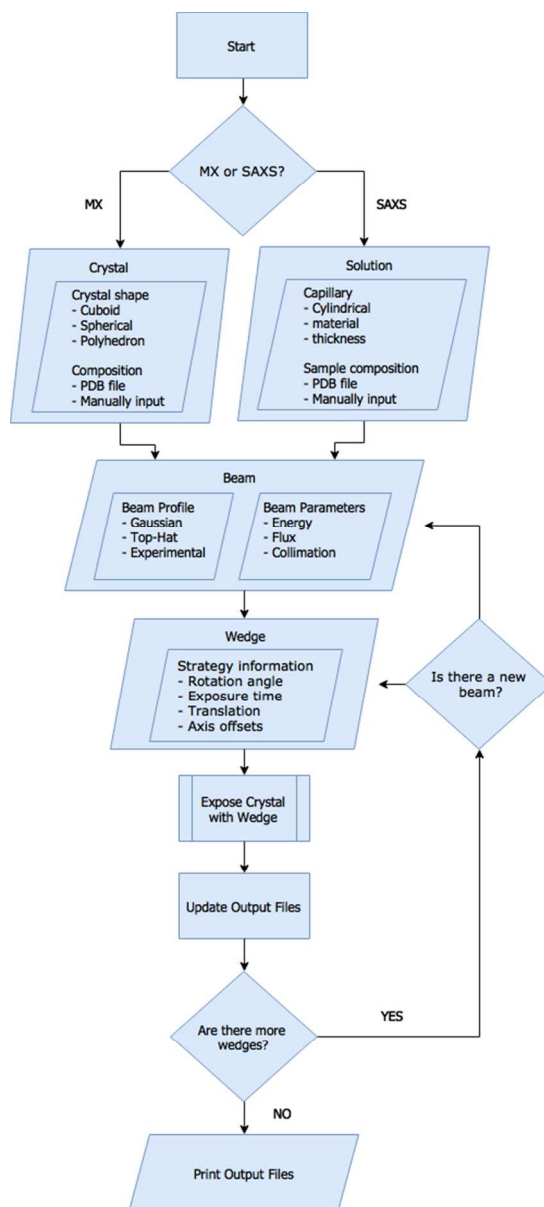


Figure 2  
Flow chart outlining the structure of RADDose-3D.

176x389mm (72 x 72 DPI)



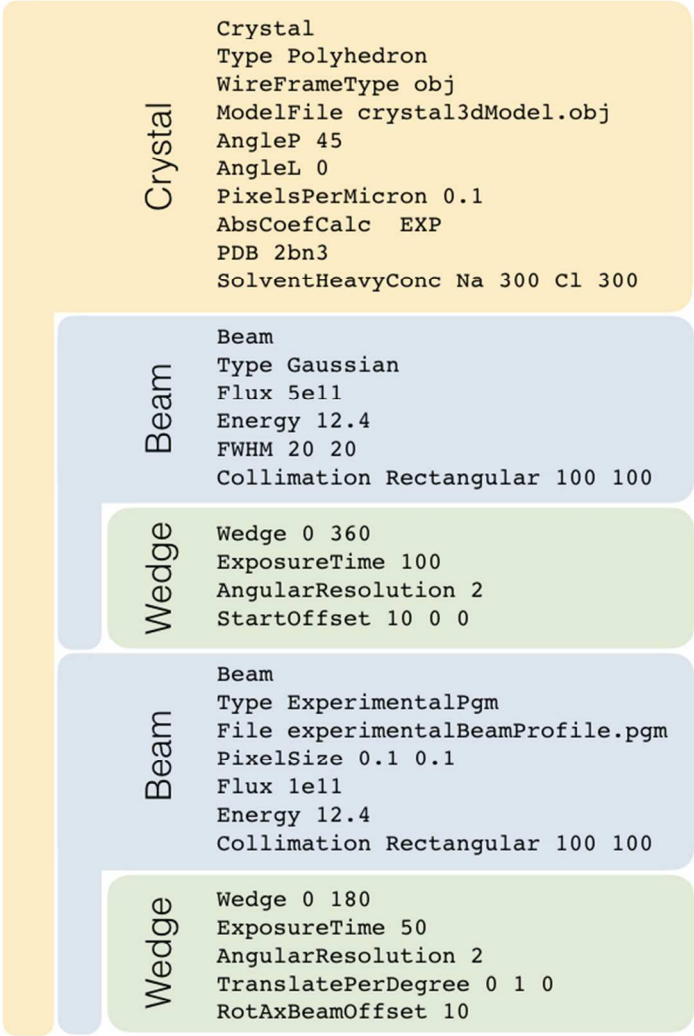


Figure 3

The structure of a typical RADDOS-3D input file. The crystal geometry and composition is first described by a 'Crystal' block (in orange). The three-dimensional geometry of the crystal has been approximated as a polyhedron (as a collection of vertices and faces) and this information has been supplied to RADDOS-3D using the 'ModelFile' flag. A 'Beam' block (in blue) followed by a 'Wedge' block (in green) describe the strategy by which the specified beam will interact with the crystal. Multiple beam and wedge parameters can be implemented in the same RADDOS-3D input file, and each exposure strategy with be run sequentially by the program. Whereas in the first beam block the beam profile will be approximated as a 2D Gaussian with FWHMs of 20  $\mu\text{m}$  x 20  $\mu\text{m}$ , in the second beam block, the beam profile has been extracted directly from the beamline and supplied to RADDOS-3D as an input .pgm file.

246x361mm (72 x 72 DPI)







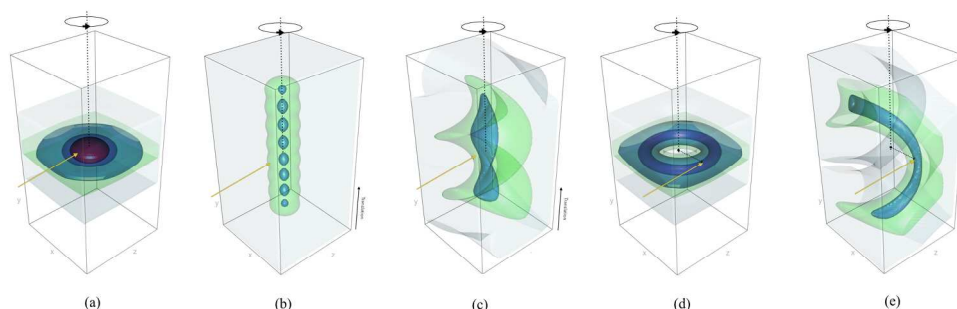


Figure 4

Effect of the dose distribution on the chosen exposure strategy modelled in RADDOSE-3D. Dose contouring levels have been shown at 0.0001 MGy (grey), 5 MGy (green), 10 MGy (light blue), 20 MGy (dark blue) and 30 MGy (red), using R ([www.r-project.org](http://www.r-project.org)). In each simulation, the crystal rotation axis (in black) and incident beam direction (in yellow, coincident with the z-axis) are shown. Unless otherwise stated, each dose distribution is generated following a 360° rotation over a total exposure time of 100 s. In (a) the crystal rotation axis and incident beam direction intersect. In (b) the crystal undergoes a series of eight 360° rotations, each lasting  $100/8 = 12.5$  s, intersected by a series of 20  $\mu\text{m}$  translations of the crystal parallel to the rotation axis to spread the dose across the crystal volume. In (c) the crystal rotation axis and incident beam direction intersect, however the crystal is continuously translated along the rotation axis at a rate of 0.2  $\mu\text{m}/^\circ$ . In (b) the crystal rotation axis has been offset by 30  $\mu\text{m}$  relative to the incident beam direction. In (e) the rotation axis is offset by 30  $\mu\text{m}$  relative to the beam direction, and the crystal is also continuously translated along the rotation axis at 0.2  $\mu\text{m}/^\circ$ . In all simulations a cuboid crystal has been modelled with dimensions  $x = 100 \mu\text{m}$ ,  $y = 200 \mu\text{m}$  and  $z = 100 \mu\text{m}$ . The beam has been modelled as Gaussian shaped (FWHM: 20  $\mu\text{m} \times 20 \mu\text{m}$ ), with energy 12.4 keV, flux  $5 \times 10^{11}$  ph/s, and a large 1 mm  $\times$  1 mm rectangular collimation in order to ensure the full crystal is continuously bathed in the beam for each simulation.

776x282mm (72 x 72 DPI)



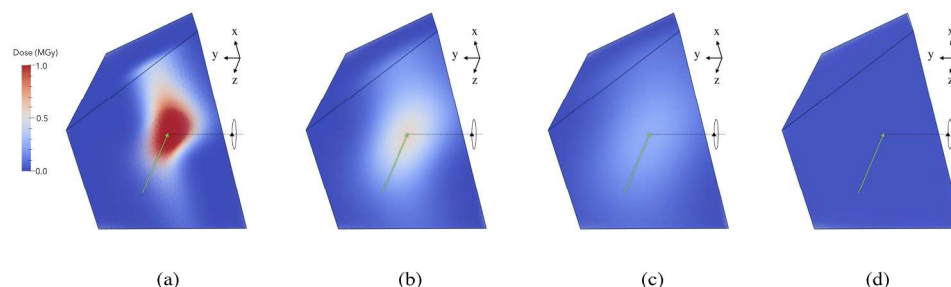


Figure 5

The effect of varying the incident beam profile on the dose distribution for an irregular polyhedron shaped crystal formed by distorting a cube of dimension  $(100\text{ }\mu\text{m})^3$  leaving the total volume the same at  $10^6\text{ }\mu\text{m}^3$ . In (a)-(c) the beam has been modelled as Gaussian shaped, and the FWHM has been varied as: (a)  $20\text{ }\mu\text{m} \times 20\text{ }\mu\text{m}$ , (b)  $40\text{ }\mu\text{m} \times 40\text{ }\mu\text{m}$  and (c)  $60\text{ }\mu\text{m} \times 60\text{ }\mu\text{m}$ . In (d) a uniform 'top-hat' shaped beam distribution has been modelled. All other beam parameters have been kept constant (energy: 12.4 keV, flux  $5 \times 10^{11}\text{ ph/s}$ , rectangular collimation:  $200\text{ }\mu\text{m} \times 200\text{ }\mu\text{m}$ ). In all simulations the crystal has been exposed for 100 s throughout a  $360^\circ$  rotation about the y-axis (shown in each plot). The direction of incident beam with respect to the initial orientation of the crystal has been shown (green arrow). The crystal morphology has been specified with the 'Type Polyhedron' flag in the RADDose-3D input file. Visualisation has been produced using the open source Paraview software package (<https://www.paraview.org>).

846x381mm (72 x 72 DPI)



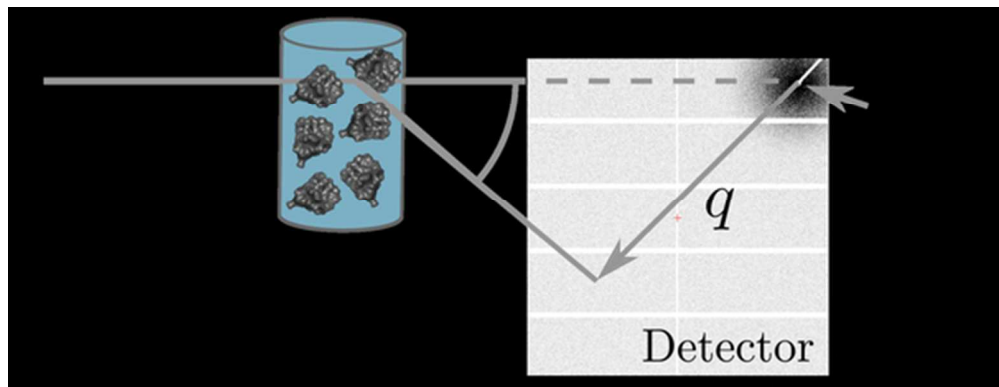


Figure 6

Diagram of a basic SAXS experiment. An X-ray beam (typical energies range between 7 and 12.5 keV) is incident on a protein SAXS sample. Commonly the sample volume exposed to the beam is between 15 – 30  $\mu\text{l}$ , with a protein concentration that usually ranges from 0.5 – 10 mg/ml. The scattered radiation is collected on a detector. The symbol,  $q$  in the figure, is termed the momentum transfer and is defined as  $q=4\pi \sin \theta/\lambda$  where  $\theta$  is half the scattering angle, and  $\lambda$  is the wavelength of the incident X-ray beam. The detector images that are generated from the experiment can be processed and analysed to determine the overall shape and size of the protein molecule in the SAXS sample.

51x19mm (300 x 300 DPI)



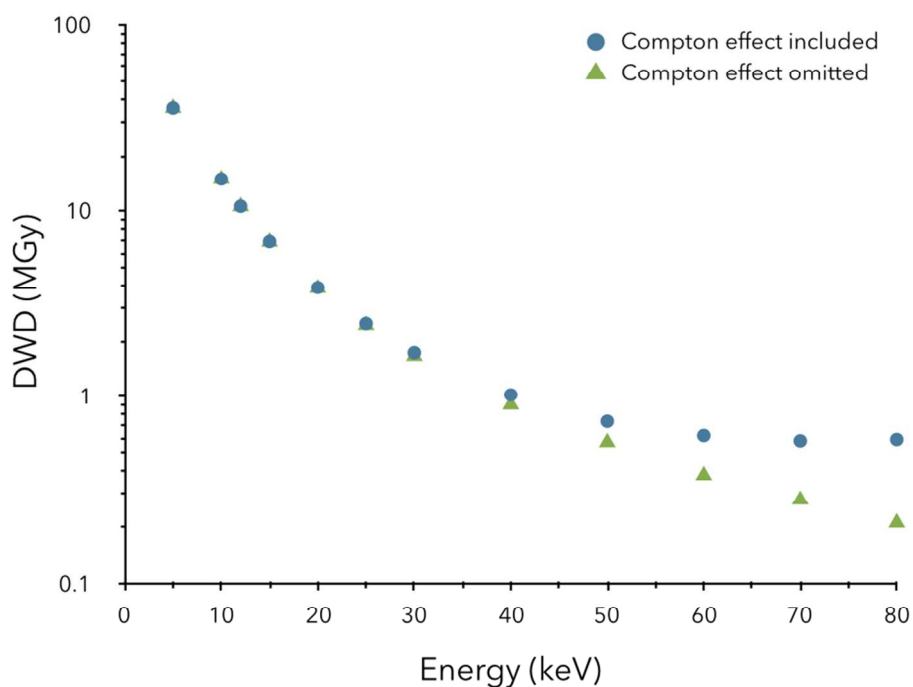


Figure 7

The effect of Compton scattering on the calculated DWD (MGy) values for a 100  $\mu\text{m}$  x 100  $\mu\text{m}$  x 100  $\mu\text{m}$  cuboid crystal in RADDOSE-3D with varying incident photon energy,  $E_x$  (keV). In all simulations, the beam has been modelled as Gaussian shaped with energy: 12.4 keV, flux:  $5 \times 10^{11}$  ph/s, FWHM: 20  $\mu\text{m}$  x 20  $\mu\text{m}$  and with a rectangular collimation size of 100  $\mu\text{m}$  x 100  $\mu\text{m}$ . In all simulations the crystal has been exposed for 100 s over a 360° rotation. Note the y-axis logarithmic scale.

361x270mm (72 x 72 DPI)



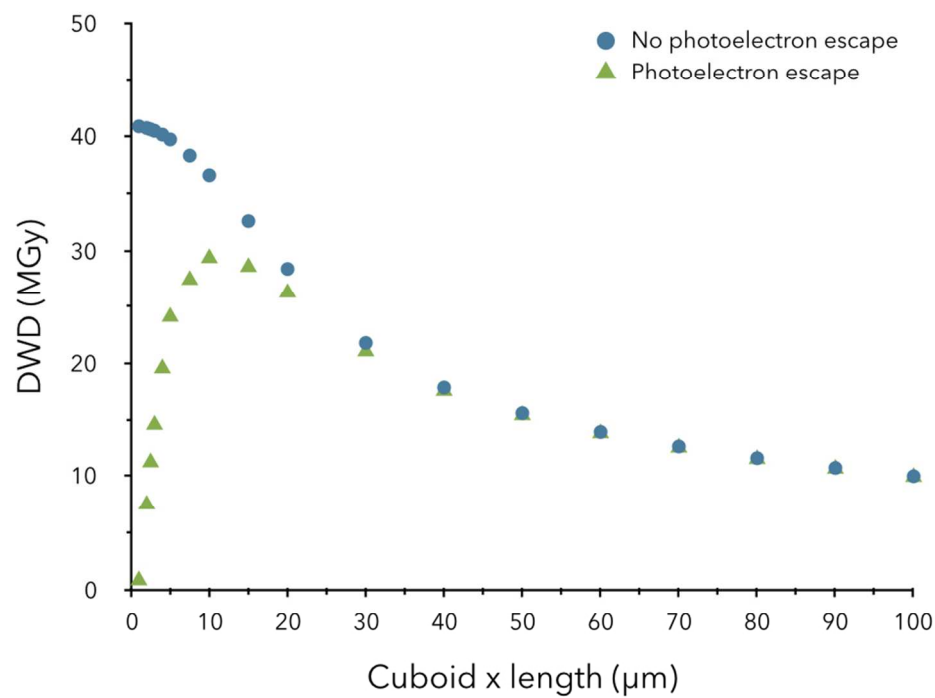


Figure 8  
The effect of accounting for photoelectron escape in RADDOS-3D on the calculated DWD (MGy) values for a various sized cubic shaped crystals. In all simulations, the beam has been modelled as Gaussian shaped with energy: 12.4 keV, flux:  $5 \times 10^{11}$  ph/s, FWHM:  $20 \mu\text{m} \times 20 \mu\text{m}$  and with a rectangular collimation size of  $100 \mu\text{m} \times 100 \mu\text{m}$ ., and the crystal has been exposed for 100 s over a  $360^\circ$ . The PixelsPerMicron parameter in RADDOS-3D has been varied for the x-dimension of each crystal (between 0.5 and 10 pixels/ $\mu\text{m}$ ) to account for the diminishing size of the crystal.

361x270mm (72 x 72 DPI)



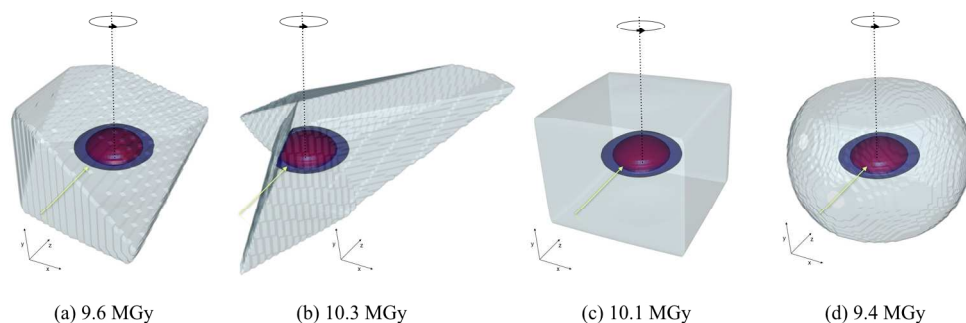


Figure 9

The effect of modelled crystal geometry on the calculated DWD (MGy) values has been illustrated for four crystal shapes, each with a total volume of  $10^6 \mu\text{m}^3$ . Dose isosurfaces are contoured at 0.001 MGy (light blue), 20 MGy (dark blue) and 30 MGy (red), using R ([www.r-project.org](http://www.r-project.org)). In (a) and (b), two irregular polyhedron-shaped crystals were generated using the open-source three-dimensional graphics software called Blender. In (c) and (d) the 'Type cuboid' and 'Type spherical' input file parameters to RADDOS-3D have been used to model the crystal as a  $100 \mu\text{m} \times 100 \mu\text{m} \times 100 \mu\text{m}$  cuboid, and  $124.2 \mu\text{m}$  diameter sphere, respectively. In all simulations, a Gaussian beam ( $12.4 \text{ keV}$ ,  $1 \times 10^{11} \text{ ph/s}$ ) was modelled with FWHM of  $20 \mu\text{m} \times 20 \mu\text{m}$ , in order to obtain the infamous 'fried egg' effect.

740x335mm (72 x 72 DPI)